Department of Engineering Physics and Mathematics
Helsinki University of Technology
02015 Espoo, Finland

# CARBON NANOTUBE SINGLE-ELECTRON DEVICES AT AUDIO AND RADIO FREQUENCIES

**Leif Roschier**

Low Temperature Laboratory

Dissertation for the degree of Doctor of Technology to
be presented with due permission for public examination
and debate in Auditorium F1 at the Helsinki University
of Technology on the 1st of June, at 12 noon

Espoo 2004

Distribution:
Helsinki University of Technology
Low Temperature Laboratory
P.O. Box 2200
FIN-02015 HUT
Tel. +358-9-451-5795
Fax. +358-9-451-2969
E-mail: Leif.Roschier@iki.fi
This dissertation can be read at http://lib.hut.fi/Diss/



ISBN 951-22-7096-X
ISBN 951-22-7097-8 (pdf)

Otamedia Oy
Espoo 2004

| HELSINKI UNIVERSITY OF TECHNOLOGY<br>P.O. BOX 1000, FIN-02015 HUT<br>http://www.hut.fi | ABSTRACT OF DOCTORAL DISSERTATION |
|---|---|

Author Roschier, Leif Robert

Name of the dissertation

CARBON NANOTUBE SINGLE-ELECTRON DEVICES AT AUDIO AND RADIO FREQUENCIES


| | |
|---|---|
| Date of manuscript 15.12.2003 | Date of the dissertation 1.6.2004 |
| ☐ Monograph | ☑ Article dissertation (summary + original articles) |
| Department | Department of Engineering Physics and Mathematics |
| Laboratory | Low Temperature Laboratory |
| Field of research | Experimental condensed-matter physics |
| Opponent(s) | Prof. Martin N. Wybourne |
| Supervisor | Prof. Martti M. Salomaa |
| (Instructor) | Prof. Pertti J. Hakonen |



Abstract

A single-electron transistor is the most sensitive charge detector known today. It is formed by a small piece of a conductor coupled to electrodes by tunnel junctions. At low frequencies, the charge sensitivity is limited by the 1/f-noise. The use of a radio-frequency modulation technique allows a wide operational bandwidth with negligible 1/f-noise contribution.

In this Thesis, a multiwalled carbon nanotube brought to contact with metal electrodes was demonstrated to work as a single-electron transistor. A scanning probe manipulation scheme was developed and it was used to fabricate the sample. The manipulation scheme was also employed to construct more complicated electronic carbon nanotube devices. It was shown that it is possible to construct a multiwalled carbon nanotube single-electron transistor having an equal to, or even higher charge sensitivity than a typical metallic device. The transmission-line parameters of the multiwalled carbon nanotube were estimated by using the environment-quantum-fluctuation theory.

The radio-frequency single-electron transistor setup was analyzed in depth and a simplified engineering formula for the charge sensitivity was derived. A radio-frequency single-electron transistor setup using a multiwalled carbon nanotube single-electron transistor was demonstrated in the built cryogenic high-frequency measurement system. A low-temperature high-electron-mobility-transistor amplifier was designed and built for the system. Measurements of the amplifier indicated a noise temperature of three Kelvins.



| | |
|---|---|
| Keywords | electron transport in mesoscopic systems, carbon nanotubes, high-frequency techniques |
| UDC 621.382.3:538.91:539.2 | Number of pages 42 |
| ISBN (printed) ISBN 951-22-7096-X | ISBN (pdf) ISBN 951-22-7097-8 |
| ISBN (others) | ISSN |
| Publisher Otamedia Oy | |
| Print distribution | |
| ☑ The dissertation can be read at http://lib.hut.fi/Diss/ | |

# Acknowledgements

DURING this research, there have been numerous individuals who have had impact to this Thesis over the years. The Thesis was was carried out in the Low Temperature Laboratory at the Helsinki University of Technology. First of all, I wish to thank director Mikko Paalanen and my supervisor Prof. Pertti Hakonen. My research is according to their vision and research budget. Prof. Martti Salomaa deserves thanks for using his time to help to complete formally this Thesis.

I am also grateful for the former and present members of the NANO group: Michel Martin, Jari Penttilä, René Lindell, Ülo Parts, Mika Sillanpää, Tero Heikkilä, Reeta Tarkiainen, Sami Lähteenmäki, Markus Ahlskog, Edouard Sonin, Janne Antson, Julien Delahaye, Takahide Yamaguchi, David Schäfer, Lasse Aaltonen and Jani Högman. I also owe thanks for Prof. Wang Taihong, whose visit was very profitable.

I was honored to work with great fellow students: Juha Martikainen, Rob Blaauwgeers, Tauno Knuuttila, Jaakko Ruohio, Roch Schanen, Juha Kopu, Risto Hänninen, Janne Viljas, Kirsi Juntunen, Vesa Norrman, Jani Kivioja, Mika Seppä, Kimmo Uutela, Jussi Toppari and Antti Finne.

The visits to Yale University were enjoyable, due mostly to the great scientists and friends: Prof. Rob Schoelkopf, Konrad Lehnert, Prof. Dan Prober, Irfan Siddiqi, Lafe Spietz and John Teufel. I was happy to use samples produced by the Chalmers group, thanks are due to: Prof. Per Delsing and Kevin Bladh.

Most of my nanotube work deserves a gratitude for the University Montpellier group for producing the materials: Catherine Journet and Prof. Patrick Bernier.

VTT–Technical Research Centre of Finland has been a long-term partner with the Low Temperature Laboratory, thanks are due to: Mikko Kiviranta,

Unto Tapper, Bertrand Schleicher and Prof. Esko Kauppinen.

The staff in the Low Temperature Laboratory is the backbone for the research infrastructure. They carry out very essential work, but seldom get any merit. I am grateful for all of You: Kari Rauhanen, Pirjo Kinanen, Juhani Kaasinen, Sami Lehtovuori, Markku Korhonen, Seppo Kaivola, Antti Huvila, Liisi Pasanen, Satu Pakarinen, Arvi Isomäki, Teija Halme, Antero Salminen, Tuire Koivistoa and Marja Holmström.

My parents Seija and Nils-Robert deserve an expression of my debt of gratitude for their support during all these years. I am grateful for my sister Solveig and brother-in-law Martti for all their help.

Finally, I would like to thank Elina for her loving support during these years of my Thesis.

Otaniemi, December 2003

Leif Roschier

# Contents

# List of abbreviations

| | |
|---|---|
| AC | alternating current |
| AFM | atomic force microscope |
| CNT | carbon nanotube |
| DC | direct current |
| MWNT | multiwalled carbon nanotube |
| PMMA | polymethyl methacrylate |
| PMMA/MAA | methyl methacrylate and methacrylic acid |
| RF | radio frequency |
| RF-SET | radio-frequency single-electron transistor |
| SET | single electron transistor |
| STM | scanning tunneling microscope |
| TRL | through-reflect-line |
| pHEMT | pseudomorphic high electron mobility transistor |

# Appended papers

This Thesis is based on the following original publications.

AFM MANIPULATION AND CARBON NANOTUBES

**[P1]** M. Martin, L. Roschier, P. Hakonen, Ü. Parts, M. Paalanen, B. Schleicher, and E. I. Kauppinen, *Manipulation of Ag nanoparticles utilizing noncontact atomic force microscopy*, Applied Physics Letters **73**, 1505 (1998).

A scheme was reported for moving metallic aerosol particles on a silicon dioxide surface using an atomic force microscope in non-contact mode. The main advantage of the scheme developed was the possibility to track the particle position in-situ.

**[P2]** L. Roschier, J. Penttilä, M. Martin, P. Hakonen, M. Paalanen, U. Tapper, E.I. Kauppinen, C. Journet, and P. Bernier, *Single-electron transistor made of multiwalled carbon nanotube using scanning probe manipulation*, Applied Physics Letters **75**, 728 (1999).

A single electron transistor, with charging energy of 24 K, was manufactured from a multiwalled carbon nanotube using scanning probe manipulation in the non-contact mode. The device was measured and characterized at sub-Kelvin temperatures. A Coulomb staircase model was employed to explain the data.

**[P3]** M. Ahlskog, R. Tarkiainen, L. Roschier, and P. Hakonen, *Single-electron transistor made of two crossing multiwalled carbon nanotubes and its noise properties*, Applied Physics Letters **77**, 4037 (2000).

A nanotube-gated, three-terminal single electron transistor was manufactured by pushing a multiwalled nanotube on top of another one

by using an atomic force microscope. The charge sensitivity of the lower nanotube was measured and the value was found to be of the same order of magnitude as that for a typical metallic single-electron transistor.

[**P4**] L. Roschier, R. Tarkiainen, M. Ahlskog, M. Paalanen, and P. Hakonen, *Multiwalled carbon nanotubes as ultrasensitive electrometers*, Applied Physics Letters **78**, 3295 (2001).

Ultra-high charge sensitivity was measured for an atomic-force-microscope manipulated, free-hanging multiwalled carbon nanotube single-electron transistor. In this configuration, the $SiO_x$ substrate is 17 nm below the nanotube and this separation is believed to be the main reason for the enhanced charge sensitivity compared to typical SETs, where the island is in direct contact with the substrate.

[**P5**] R. Tarkiainen, M. Ahlskog, J. Penttilä, L. Roschier, P. Hakonen, M. Paalanen, and E. Sonin, *Multiwalled carbon nanotube: Luttinger versus Fermi liquid*, Physical Review B **64**, 195412 (2001).

Tunnelling conductance at high voltages was used to determine the transmission-line parameters of the arc-discharge-grown multiwalled carbon nanotube samples. The fits yield a characteristic impedance of 1.3–7.7 k$\Omega$ and kinetic inductance of 0.1–4.2 nH/$\mu$m for the measured samples.

[**P6**] L. Roschier, J. Penttilä, M. Martin, P. Hakonen, M. Paalanen, U. Tapper, E.I. Kauppinen, C. Journet and P. Bernier, *Transport studies of multiwalled carbon nanotubes utilizing AFM manipulation*, In C. Glattli, M. Sanquer and J. Trân Thanh Vân, editors, Quantum Physics at Mesoscopic Scale, p. 25, Proc. of the XXXIVth Recontres de Moriond, EDP Sciences, (2000).

Transport measurements of the multiwalled carbon nanotube single-electron transistor are discussed. The measured differential conductance probes the density of states.

[**P7**] M. Ahlskog, P. Hakonen, M. Paalanen, L. Roschier, and R. Tarkiainen, *Multiwalled carbon nanotubes as building blocks in nanoelectron-*

*ics*, Journal of Low Temperature Physics **124**, 335 (2001)

A review of our measurements on multiwalled carbon nanotubes emphasizing their use as electrical components. Atomic-force-microscope manipulated multiwalled carbon nanotubes are shown to work as single-electron transistors at 4.2 K. Reactively ion-etched nanotubes produced by chemical vapor deposition are shown to work as small size resistors with the large resistivity of 100 k$\Omega/\mu$m.

RF-SET AND HIGH FREQUENCY AMPLIFIER

[**P8**] L. Roschier, P. Hakonen, K. Bladh, P. Delsing, K.W. Lehnert, L. Spietz, and R.J. Schoelkopf, *Noise performance of the radio frequency single-electron transistor*, Journal of Applied Physics **95**, 1274 (2004).

Theoretical analysis and experiments were carried out to estimate the charge sensitivity of a radio frequency single-electron transistor. The theoretical prediction is based on a model which includes equivalent circuits for all the components of the measurement system. First-stage-amplifier was involved in the analysis and the noise power wave formalism was employed in the analysis of the aluminum single-electron transistor test system.

[**P9**] L. Roschier and Pertti Hakonen, *Design of cryogenic 700 MHz HEMT amplifier*, TKK report, TKK-KYL-010, (2004).

A cryogenic high frequency amplifier was designed and tested. The design process involved the use of cryogenic $S$-parameters that were measured with the help of a TRL-calibration method. The tested amplifier showed a noise temperature of three Kelvins.

# Author's contribution

Most of the research work discussed in this Thesis was performed in the NANO group in the Low Temperature Laboratory at the Helsinki University of Technology. The research discussed in publication [P8] was done in collaboration with Yale University and Chalmers University of Technology.

The NANO group was founded 1996 and I was one of the first students recruited in 1997. I was heavily involved in setting up the research infrastructure, i.e., recipes for sample fabrication, cryostats for refrigeration and measurement system buildup including computer routines for data collection and analysis. During the first years I was involved in the development of the atomic-force-microscope manipulation techniques [P1]. I employed the method to make a single-electron transistor out of a multiwalled carbon nanotube [P2]. Later, I started to design a RF-SET measurement system. The last couple of years I spent building the refrigeration and measurement setup for the experiments that use high-frequency read-out techniques. I also designed the cryogenic amplifier for the system [P9]. From my visits to Yale University in 2000 and 2001 emerged the RF-SET sensitivity analysis [P8].

I have been participating in all of the measurements for publications [P1, P2, P4–P9]. In publication [P3] I participated in the sample-fabrication process. I have taken part into the writing process of publications [P1, P4] by reading manuscripts, preparing pictures and analyzing data. Publications [P2, P6, P8, P9] were largely measured, analyzed and written by me.

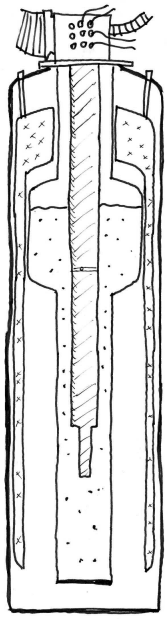

# Chapter 1

# Introduction

THE main topics of this Thesis are single electronics, particularly the radio-frequency single-electron transistor (RF-SET), and multiwalled carbon nanotubes (MWNT). Single electronics as a branch of science may be considered almost twenty years old. The first single-electron transistor (SET) was demonstrated experimentally in 1987 [1]. Carbon nanotubes were discovered over ten years ago [2]. The latest topic, the readout technique named RF-SET, was invented five years ago [3, 4]. During my experimental thesis work these blocks were combined and an experimental high-frequency mK-setup was constructed and a MWNT RF-SET was demonstrated. As a practical by-product, an atomic-force-microscope manipulation scheme was developed and a cryogenic high-frequency amplifier was designed and built.

## 1.1 Coulomb blockade and single electronics

Single-electron devices are based on the effect of Coulomb blockade. In this effect, tunnelling of a single electron through a tunnel junction with capacitance $C$ is suppressed at voltages $V < e/2C$, because otherwise electrostatic energy would increase: $C(V \pm e/C)^2 > CV^2$ [5]. The first published results of this effect in thin metal films date back to the 1950's [6] and 1960's [7]. Observation of this effect requires $kT < E_C$. That is, smearing due to thermal fluctuations $kT$ has to be smaller than the charging energy $E_C = e^2/2C$.

Figure 1.1a illustrates a single-electron transistor (SET). A SET is formed by connecting an "island" to a gate electrode capacitively and to the drain

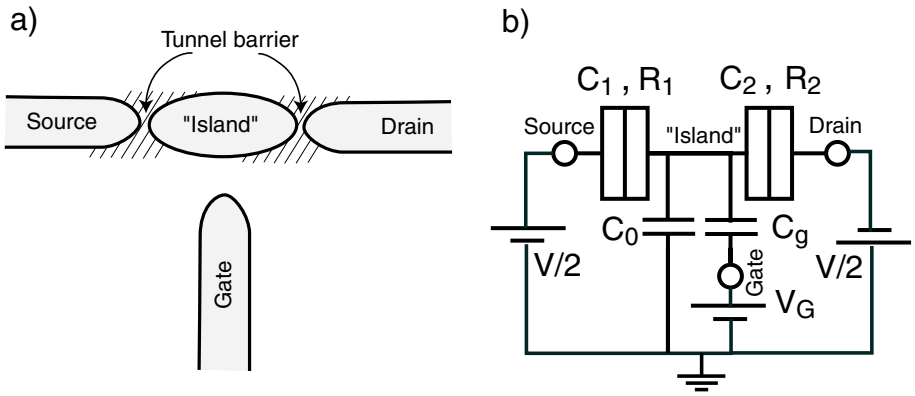


Figure 1.1: a) SET geometry. An island is connected to the drain and source electrodes via tunnel barriers. A separate gate electrode controls the island potential. b) The electric schema of the SET and the voltage sources. Tunnel junctions are characterized by their capacitances $C_i$ and resistances $R_i$, $i = 1, 2$. The gate electrode couples to the island capacitively with the capacitance $C_g$. The charging energy $E_C = e^2/2C_\Sigma$ of the SET is the sum of all island capacitances $C_\Sigma = C_1 + C_2 + C_g + C_0$. $C_0$ is the self-capacitance of the island and it is often negligible compared to the tunnel junction capacitances.

and source electrodes via tunnel junctions having tunnel resistances $R$ higher than $h/4e^2 \approx 6.5$ kΩ [8]. This relation ensures that the charging energy $E_C$ is larger than the scale of quantum fluctuations [9]. In this configuration the total island charge may change only by tunnelling of single electrons with charge $-e$ [8]. By considering classical electrostatic energy difference $\Delta E = (Q_0 - (n+1)e)^2/2C_\Sigma - (Q_0 - ne)^2/2C_\Sigma$ of adding a single electron to the island and by taking into account the work done by the voltage sources, one finds the regions for the blockade of the current [10]

$$e\Big(n + \frac{1}{2}\Big) > C_g V_g + VC_1 + Q_0 > e\Big(n - \frac{1}{2}\Big)$$

$$e\Big(n + \frac{1}{2}\Big) > C_g V_g - VC_2 + Q_0 > e\Big(n - \frac{1}{2}\Big). \tag{1.1}$$

$Q_0$ is the background charge of the island, a slowly varying continuous offset for the integer number $n$ of electrons on the island. The physical sense of this charge is the following. It is the continuous polarization charge of the island which is bound by the gate field and is taken out of the energy balance of the tunnel junctions [8]. Figure 1.2 illustrates the regions of Coulomb blockade.

As an example of conductance measurements, data on a MWNT SET [P3] is illustrated in Fig. 1.3.

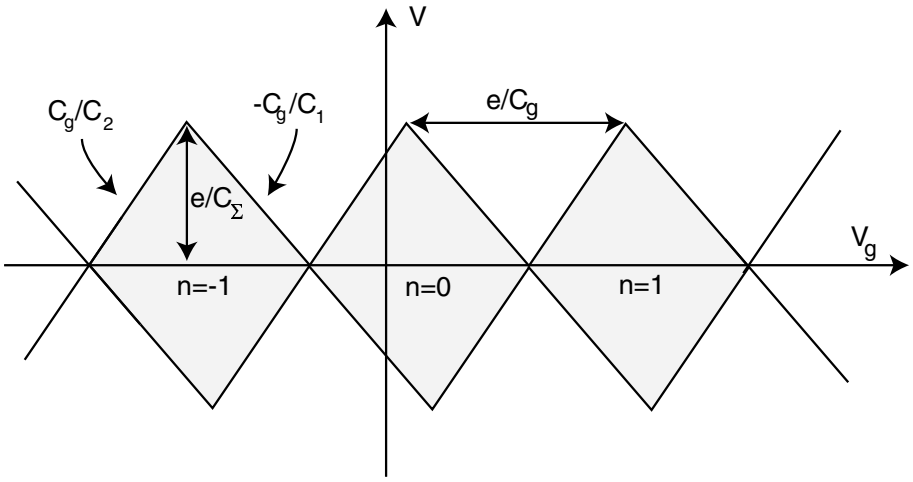


Figure 1.2: Stability diagram of a SET. Regions of Coulomb blockade are denoted by rhombic-shape gray areas that are also called the Coulomb-charging diamonds. The slopes and the periods of the diamonds are set by the capacitances $C_1$, $C_2$ and $C_g$, as stated in Eq. (1.1).

The SET operation as a transistor is due to the varying gate charge $V_g C_g$ that controls the device conductance between zero and finite conductivity, as can be seen in Fig. 1.2. A SET is a charge amplifier or a charge-to-power transducer. Usual metallic SETs can detect a charge variation of $3{\times}10^{-4} e/\sqrt{\text{Hz}}$ at 10 Hz [11]. Results of Ref. [P4] demonstrate that in a carbon nanotube SET the charge sensitivity may be higher by a factor $\sim$ 10, presumably due to the increased distance of the island from the charge fluctuators residing in the $SiO_x$ substrate.

If the SET is asymmetrically current biased, its voltage gain is $\sim C_g/C_1$ and one needs a large gate capacitance in order to obtain a voltage gain over unity [12]. The best commercial, room-temperature voltage amplifiers based on field-effect-transistors (FET) have a voltage noise of $\sim$ 1 nV/$\sqrt{\text{Hz}}$ [13]. A SET with a similar voltage noise requires at most a charge noise of $10^{-5}$ e/$\sqrt{\text{Hz}}$ using $\delta V = \delta q/C_g$ and $C_g = 1$ fF. In practice, it is very hard to fabricate a metallic SET having this charge noise level at low frequencies due to the $1/f$-noise. The conclusion is that a metallic SET is an impractical

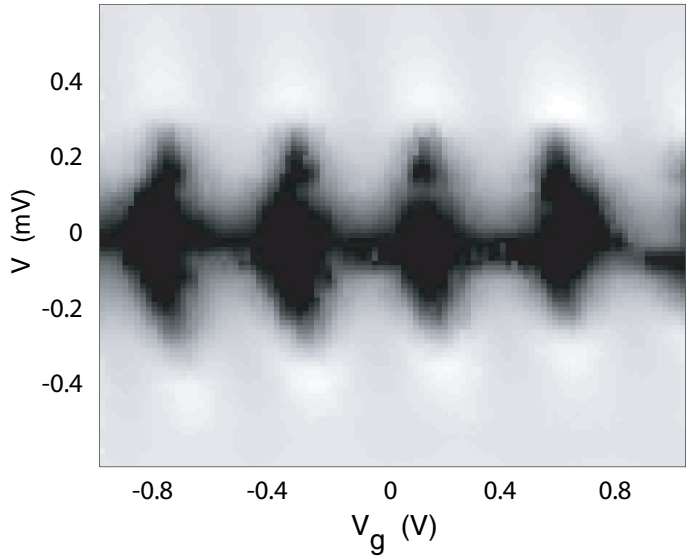


Figure 1.3: Differential conductance in a logarithmic scale of the MWNT sample discussed in Ref. [P3] . The Coulomb charging diamonds are visible. Lighter color means higher conductance.

general purpose voltage amplifier, but a superior electrometer.

## 1.2 SET read-out techniques

At low frequencies, close to DC there are two prevailing ways to read out a charge signal detected by the SET. One way is to voltage bias the SET and to measure the current that depends on the island charge. The other choice is to current bias the SET and to measure the voltage. In both cases, the maximum signal bandwidth is set by the $RC$ time, where $R$ is the SET resistance and $C$ is the shunting capacitance of the measurement leads. With the practical values of the shunting capacitance $C \sim 0.1$ nF and a SET resistance of $\sim$ 50–200 k$\Omega$, the bandwidth is at most on the order of 100 kHz. In 1998, it was demonstrated that a SET may be read with an increased bandwidth $\sim$ 100 MHz. Instead of reading voltage or current, the power dissipation was read. Also a better charge sensitivity was proved at high frequencies, where the $1/f$-noise did not set the noise floor as in the case of the DC measurements [3, 4]. The measurement setup was named a radio-

frequency single-electron transistor (RF-SET).

## 1.3 Amplifiers

The first issue that an experimental physicist has to consider when designing an experiment is the level of the signal compared with the level of perturbations. Often these perturbations are called noise, even though sometimes the term refers to the signal revealing information about the test system. In this Thesis, the term *noise* means perturbations, limitations to the accuracy to read the desired coherent signal. In order to extract information from the system under study, it has to be attached to a measuring device which introduces two interfering effects;(i) It adds noise to the measured parameter of the system, and (ii) it perturbs or back-acts the system measured. In order to minimize these perturbations, a low-noise amplifier is employed as the first device attached to the test system.

Ordinarily amplifiers are treated as linear devices in electric measurements. That is, they are described by a set of $2 \times 2$ complex matrices that, for instance, relate the currents and voltages between the input and output ports at a specific frequency. For this purpose, there is a freedom to choose not more than two complex numbers to describe the noise properties of the linear amplifier. An exemplary set of these four noise parameters are the real amplitudes of the voltage and current noise sources at the amplifier input and their complex correlations [14]. Often, low-frequency amplifiers are specified using only the amplitudes of the voltage and current noise generators and the complex correlation coefficient between the amplitudes is assumed to be negligible.

The noise temperature $T_0$ of an amplifier is defined in such a way that the exchangeable noise power at the amplifier output is the same with a noiseless input impedance $Z$ and the noisy amplifier or with an input impedance at a physical temperature $T_0$ and a noiseless amplifier [15]. It follows that there is an optimum $Z$, a noise match, that yields the lowest $T_0$ [14]. The minimum detectable signal power from a sample in a band of 1 Hz is $\sim k_B T_0$ if the amplifier is the dominating noise source. In the state-of-the-art commercial low-frequency amplifiers ($f \lesssim 100$ kHz) operating at room temperature, the noise temperature is on the order of one Kelvin. At the

higher frequencies of around 1 GHz, cryogenic cooling is required to achieve the lowest noise temperature of a few Kelvins [16]. Another reason for the cryogenic operation for high-frequency amplifiers is the consequence of the fact that signal losses in warm coaxial cables in front of an amplifier increase its noise temperature significantly. As an example, an amplifier with $T_0 =$ 1 K and 3 dB attenuation at the input cable at the temperature of 150 K is effectively an amplifier with $T_0 \sim$75 K [17]. A fundamental limit for the noise temperature of a phase-insensitive amplifier is set by the quantum fluctuations: $T_0 \geq \hbar\omega/2$ [18], that is ∼25 mK at $\omega/2\pi = 1$ GHz. Thus noise temperatures of the present GHz-amplifiers need to decrease by two orders of magnitude in order to reach the fundamental limit.

The signal power in a typical Al sample RF-SET, corresponding to a charge of a single electron $e$ is on the order of –90 dBm in front of the first pre-amplifier. Here $x$ dBm equates $10^{x/10}$ mW. The noise power of an amplifier with $T_0 = 4$ K is –192 dBm in a band of 1 Hz. From these simple order-of-magnitude estimates it follows that the charge sensitivity limited by the amplifier noise is $\sim 10^{-5}$ e/$\sqrt{\text{Hz}}$. The internal shot-noise limit of a typical RF-SET is $\sim 10^{-6}$ e/$\sqrt{\text{Hz}}$ [19]. One needs a sub-Kelvin noise temperature amplifier in order to reach the internal limit of the RF-SET.

## 1.4 Carbon nanotubes

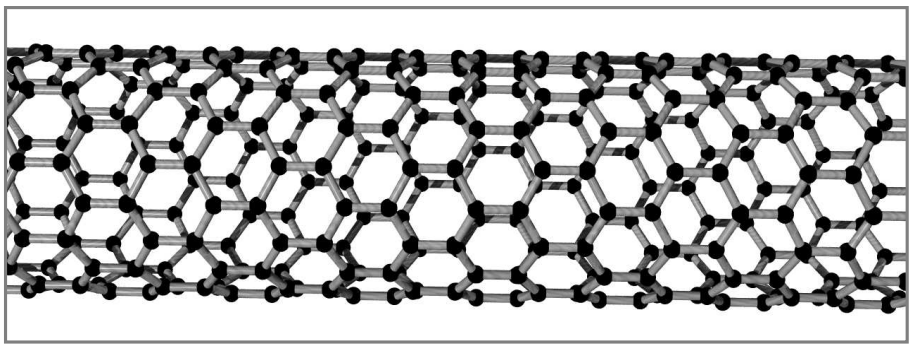

Figure 1.4: Carbon nanotube (10,0).

Graphite is a 3D layered hexagonal lattice of carbon atoms. A single layer is called a graphene sheet [20]. Carbon nanotubes (CNTs) may be

considered as graphene sheets wrapped into the form of a cylinder. There are two types of CNTs: Singlewalled CNTs consist of a single cylinder while multiwalled nanotubes (MWNT) are formed of many concentric tubes inside each other. Since the discovery of the CNTs [2], they have attracted a considerable amount of scientific interest. Some of the many electrical properties experimentally investigated in CNTs are, e.g., the band structure [21, 22], single charging effects [23], Kondo effect [24], ballistic conduction [25, 26], proximity-induced [27] and intrinsic superconductivity [28], $1/f$-noise [29] and Luttinger-liquid phenomena [30, 31, 32]. Some excellent reviews on carbon nanotubes are found, e.g., in Refs. [33, 20, 34].

## Band structure

The First articles on the band structure of singlewalled CNTs were published in 1992 [35, 36, 37], one year after their discovery. The basic principle was to employ the two-dimensional graphene dispersion relation [38], in conjunction with periodic boundary conditions around the circumference of the CNT. It turned out in this model that, depending on the chirality, the tubes are either metallic ($n - m = 3p$) or semiconducting ($n - m \neq 3p$), where $p$ is an integer [20]. The chirality indices $(n, m)$ are defined in Fig. 1.5a.

The energy-band structure was experimentally demonstrated later for singlewalled CNTs in Refs. [21, 22] using scanning tunnelling spectroscopy. However, there is in practice often a controversy between the observed electrical transport properties and a simple band picture in the measurements, where carbon nanotube is contacted to metal electrodes. This is due to the lack of control and understanding of the role of the metal contacts that play a significant role in the transport properties [39]. Also impurities and surfactants on the tube often break down the ideal picture in practical experiments [26].

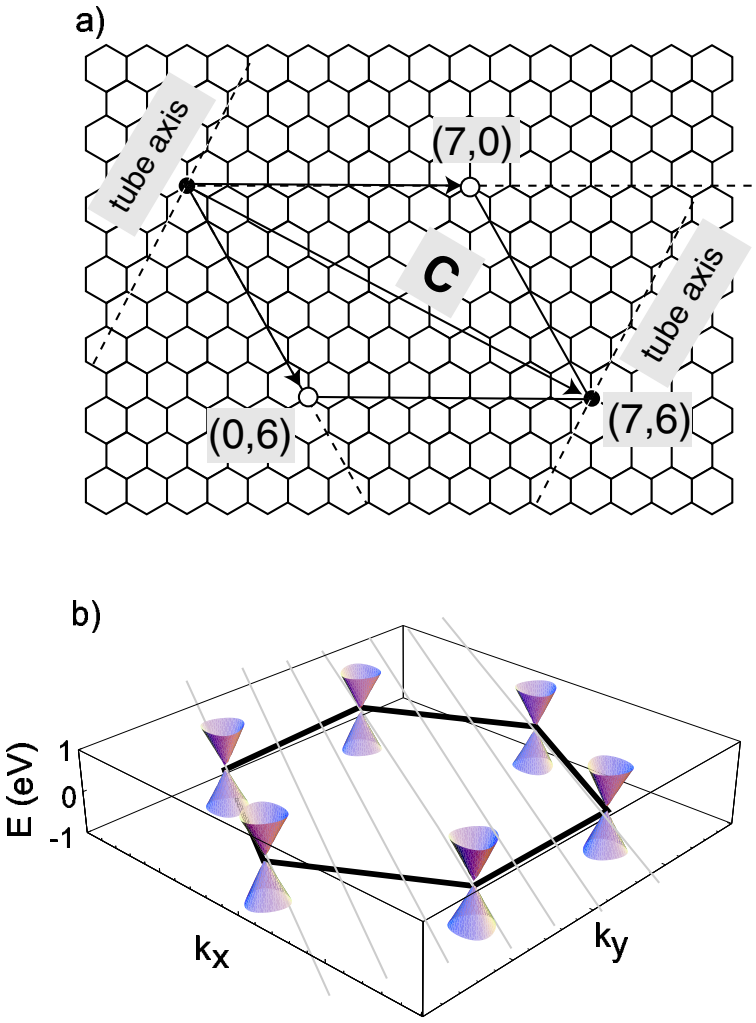


Figure 1.5: a) Hexagonal lattice of a graphene sheet. A nanotube is formed by cutting the sheet along the dashed lines and wrapping it such that the black circles coincide. The chirality indices ($n$,$m$) are defined with the help of two base vectors as illustrated. b) The band structure of graphene at low excitation energies around Fermi energy. The black hexagon denotes the first Brillouin zone in the reciprocal space. Gray lines denote the allowed wave numbers due to periodic boundary conditions for the nanotubes. Since the lines in this figure pass through the cone centers, the nanotube is metallic.

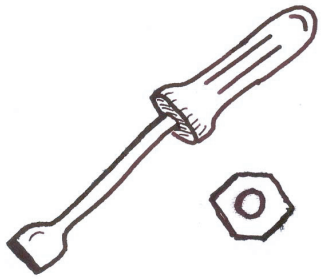

# Chapter 2

# Experimental techniques

## 2.1 Measurement setup

The experiments reported in publications [P2–P7] of this Thesis were measured using a small plastic dilution refrigerator with a base temperature of ∼80–120 mK [40]. Fig. 2.1 illustrates a typical setup for these measurements. The measurement setup for the results discussed in Ref. [P8] is discussed and displayed in Fig. 4 of the same publication.

The main task of this Thesis work was to build a cryogenic high-frequency measurement setup. The MWNT RF-SET measurements, discussed in Sec. 5.1, were measured using this setup. The cryostat is a commercial dilution refrigerator [41] reaching a base temperature of 10 mK. The photograph in Fig. 2.2 illustrates the parts of the cryostat below 4.2 K and the sample holder for the RF-SET setup.

## 2.2 Sample fabrication

The electrode structures for the MWNT samples used in the experiments were prepared using e-beam lithography. Small $5\times10$ mm$^2$ pieces of a (100) 4-inch oxidized silicon wafer were used as substrates. A typical sample-fabrication process is as follows: A bilayer resist over the silicon substrate was patterned with electron-beam lithography, by using an electron microscope

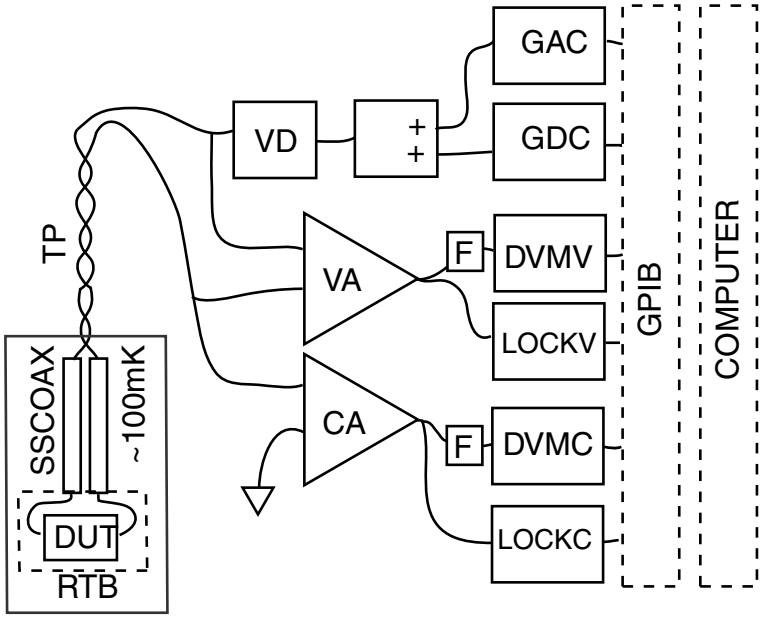


Figure 2.1: Low-frequency measurement setup. Devices corresponding to the acronyms are: GAC (voltage generator AC, HP33120A), GDC (voltage generator DC, HP33120A), VD (resistive voltage divider), TP (twisted-pair cable), SSCOX (stainless-steel coaxial cable, Philips Thermocoax), DUT (device under test), RTB (radiation tight box), VA (voltage pre-amplifier, Standford SR560), CA (current pre-amplifier, Stanford SR570 or DL Instruments 1211), DVMV (digital voltmeter for voltage, HP34401A), DVMC (digital voltmeter for current, HP34401A), LOCKV (lockin-amplifier for voltage, Stanford SR830 or EG&G 7260), LOCKC (lockin-amplifier for current, Stanford SR830 or EG&G 7260). The equipment is controlled by a computer via an optically isolated GPIB bus.

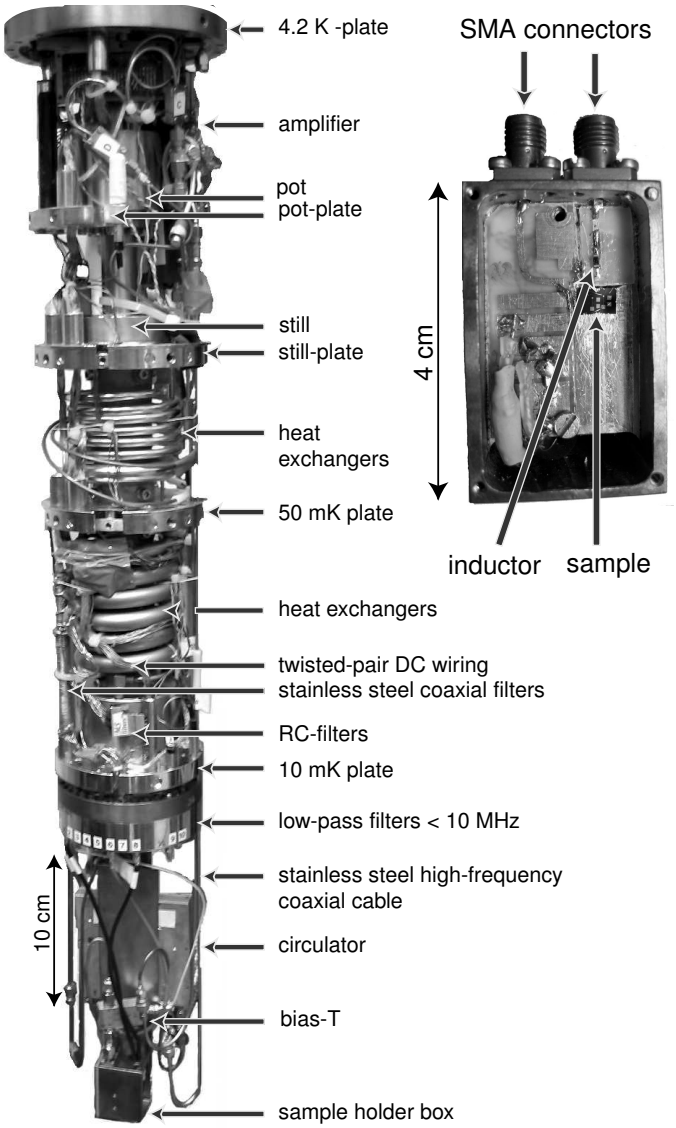


Figure 2.2: Left: Photograph of the parts of the high-frequency cryostat below 4.2 K. Unlike in most cryostats, there is a large space for components to be attached to the 10 mK plate. The cryostat has a "sliding seal" structure and all the attached components are located inside the vacuum. There is a limited space for the components that need to be attached to the 4.2 K-plate. In a typical cryostat these components are situated inside the Helium bath. Top-right: sample-holder box (without cover) used for the RF-SET measurements.

Table 2.1: Test results of vacuum brazing of MWNTs to gold electrodes in order to lower the contact resistance.

| temperature (°C) | time (s) | resistance kΩ |
|---|---|---|
| 700 | 30 | 100 |
| 700 | 40 | 10 |
| 700 | 120 | no electrodes left |
| 750 | 40 | no electrodes left |

(JEOL JSM-6400) and NPGS pattern generation software [42]. The bottom layer of the resist was PMMA/MAA (methyl methacrylate/methacrylic acid) and the top layer was PMMA. The sample was developed in methyl ethyl ketone:methyl isobutyl ketone (1:4) solution for the time of 10 s at a temperature of 17 °C. Evaporation of the electrodes was performed in an Edwards 306 Vacuum coater at a base pressure of $\sim 2 \times 10^{-6}$ mbar or in an ultra-high-vacuum chamber at a base pressure of $\sim 10^{-9}$ mbar. A sticking layer of 2 nm of chromium or titanium was evaporated before evaporation of the ∼20 nm thick layer of gold. The lift-off was carried out in acetone at room temperature. Sample resistance was lowered in Ref. [P4] to 40 kΩ by brazing the sample in quartz tube oven at 700 °C for 30 seconds. Table 2.1 displays the brazing results obtained for MWNTs manufactured by MER Corp. (type 2) [43].

## Scanning probe manipulation

The atomic force microscope (AFM)[1] was invented in 1986 [44]. It has proven to be a superior tool in the characterization of the topography of small structures. The basic principle of operation of an AFM is to use a small tip connected to a spring to sense forces between the tip and the sample. The most important force is the van der Waals force that is strong at small distances (¡ 100 nm) due to the $\propto d^{-6}$ potential dependence of the distance $d$ between the objects. In contrast to a scanning tunnelling microscope (STM) based on a tunnelling current from the conducting tip to a conducting sample, AFM

[1] AFM belongs to the class of scanning probe microscopes.

does not require a conducting substrate to operate.

For lithographic purposes, both AFM and STM provide only limited capabilities due to their sequential nature. Because of this, optical lithography as a parallel lithographic method will hardly ever be surpassed in commercial mass-applications. AFM and STM lithographies are, however, versatile tools for academic experiments. Maybe the most famous demonstration of STM for the lithographic purposes was the writing of letters by moving weakly adsorbed Xe atoms on a nickel surface [45]. The first demonstration that the AFM tip can be used for lithography was the manipulation of small aerosol particles and Au clusters in 1995 [46, 47]. These methods used the AFM in the contact mode, while pushing the objects. The idea was simply to position the tip close to the surface and to push the particle by moving the tip laterally. These methods suffered from the fact that a new image had to be taken between every push and particles sometimes got stuck to the tip. CNT manipulation using the AFM was first reported in 1997 [48]. Later, AFM has been exploited to explore interactions between a CNT and the underlying surface [49] or to probe sliding and rolling of MWNTs [50].

In 1998, it was demonstrated independently in Refs. [P1] and [51] a moving scheme, slightly different from the previous ones, utilizing AFM in the non-contact mode (NCM). The essential improvements were that particles did not any more stick to the tip and the movement of the particle could be observed in real time. Hence, the manipulation routine was substantially accelerated.

The algorithm used to move the aerosol particles in Ref. [P1] is the following: A topography image of the sample surface is taken to locate the particles. A line scan position is selected with the help of the image. The exact position of the particle is found by looking at the topography of the line-scan and by varying the line-scan position slightly. The feedback loop is turned off and the vibration amplitude of the tip is acquired from the scanned line. The tip is lowered until it touches the particle. After lowering the tip a bit more, the particle moves. The scan frequency during the manipulation was typically 30 Hz. The AFM imaging and manipulation of aerosol particles and MWNTs was performed using Autoprobe CP by Park Scientific Instruments (PSI). We used commercial boron doped silicon cantilevers (Ultralevers), manufactured by PSI, with tip radius $\sim$ 10 nm. The

cantilevers had typically force constants of 2–3 N/m. All manipulations were performed in ambient air.

In Ref. [52] it was found for the same force constant cantilevers as the ones used in our manipulations that the tip amplitude decreases linearly while approaching the surface. The tip does not "tap" or touch the surface while oscillating. Once the tip is lowered below the critical distance from the surface, it stays in touch with the surface. From the fact that the tip amplitude could be monitored *in-situ* during the aerosol particle move in our experiment [P1] , it follows that the tip does not touch the substrate surface. If it touched, it would stay in contact with the surface due to the large nonlinear van der Waals force compared to the linear cantilever force constant [52]. The tip approaches the particle vibrating and stays in touch with the particle before the particle is moved [P1] . This is visible in the vibration amplitude that does not show any wiggle when the tip is over the aerosol particle. In the manipulation of the MWNTs, the cantilever vibration most often ceased before the MWNT moved. The conclusion is that the tip stays in contact with the surface and does not vibrate in this process. The monitoring of the vibration amplitude has two functions: tracking the position of the MWNT and finding the correct tip height for the manipulation.

The MWNT samples in Refs. [P2–P4, P6, P7] were fabricated using AFM manipulation. In Refs. [P3, P4, P6], the MWNT was pushed over the gold electrodes, which were sometimes two times thicker than the MWNT diameter. The AFM manipulation typically lasted from half a day to a couple of days. The objects were moved at maximum a distance of 1–2 $\mu$m. The first move of an object always required more force than the subsequent moves. After the manipulation, the tip wore off often into useless condition for taking high quality topographic images. The original imaging software shipped with the AFM turned out to work better for the manipulation than a home-made application software.

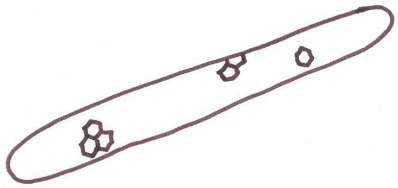

# Chapter 3

# Carbon nanotubes

THE experimental work on CNT's in this Thesis is concentrated mostly on single charging effects in CNT's. In Refs. [P2] and [P6] , a SET was manufactured from MWNT using scanning probe manipulation. In Ref. [P3] , a SET was fabricated by pushing one multiwalled nanotube on top of an other one. In Ref. [P4] noise properties of a MWNT are shown to be close to the best metallic SETs. Paper [P5] extracts transmission-line parameters of a MWNT nanotube using environment-quantum-fluctuation (EQF) theory. CNT's possibilities as building blocks in nanoelectronics are reviewed in Ref. [P7] .

## 3.1 Carbon nanotube as a transmission line

Graphene has two free $\pi$-electrons per unit cell and it is a zero gap semiconductor or semimetal. Similarly, metallic CNTs have double Fermi point degeneracy. If spin-degeneracy is included, metallic CNT is fourfold degenerate. In other words, the lowest energy band of metallic CNTs consists of four one-dimensional channels.

A single channel in a one-dimensional conductor has a density of states $n = L/2\pi\hbar v_F$, where $v_F$ is the Fermi velocity and $L$ is the length of the conductor. For CNT, the Fermi velocity is usually taken as $v_F = 8{\times}10^5$ m/s and it follows that the kinetic inductance

$$L_K = m^\star/ne^2 = \frac{h}{2e^2 v_F}, \tag{3.1}$$

due to the kinetic energy of the electrons $v_F^2/2m^\star$, is 2–3 orders of magnitude larger than the magnetic inductance $L_m \approx \mu_0 \ln(d/r)$ [53, 54]. Here $d$ is the distance of the CNT to a ground plane and $r$ the radius of the CNT.

Similarly, the density of states $n$ makes a contribution to the capacitance of the one-dimensional conductor since the spacing between the quantum states $\delta E = 1/n$ can be equated with the change in the capacitive energy $\delta E = e^2/2C_Q$, giving $C_Q = 2e^2/hv_F$ [53, 54]. This is of the same order of magnitude as the geometric capacitance per unit length $C_g \approx 2\pi\epsilon/\ln(d/r)$ for CNTs. Thus the effective capacitance per unit length is $C = (1/C_g + 1/C_Q)^{-1}$.

It is interesting to note that the wave velocity for a one-dimensional transmission line without geometric capacitance equals Fermi velocity $v_F = \sqrt{1/(L_K C_Q)}$ and the characteristic impedance $Z = L_K/C_Q = h/2e^2 = 12.5$ kΩ equals half the quantum resistance [53]. By taking into account the geometric capacitance, the wave (plasma) velocity increases to the value $v_p = \sqrt{(1/L_K)(1/C_Q + 1/C_g)}$ and the characteristic impedance to the value

$$Z = \sqrt{L_K \left( \frac{1}{C_Q} + \frac{1}{C_g} \right)}. \tag{3.2}$$

For a metallic CNT, there exists a four-fold degeneracy and the density of states is $n = 4ML\hbar v_F/2\pi$, where $M$ denotes the number of bands taking part in the conduction. The geometric capacitance couples the four degenerate channels together, and a metallic CNT may be considered as a strongly interacting one-dimensional electron system, a Luttinger liquid, that has one current-carrying mode and three neutral modes carrying spin current [53, 54]. There has been indirect experimental evidence, via power law scaling of IV-curves, that CNT's show Luttinger-liquid behavior [30, 31, 32]. It has been shown that EQF-theory also explains the measured data [54].

Ref. [P5] uses EQF [10] theory to extract transmission-line parameters of multiwalled CNTs. EQF is a theory that takes into account the effect of environment phase fluctuations into the tunnelling probability. It is shown in Ref. [55, 56] that EQF yields high-voltage IV-curve asymptotes

$$I = \frac{1}{R_T} \left( V - \frac{e}{2C_T} + \frac{R_K}{Z} \left( \frac{e}{2\pi C_T} \right)^2 \frac{1}{V} \right), \tag{3.3}$$

where $R_T$ is the tunnelling resistance, $R_K = h/e^2$ the quantum resistance and $Z$ the impedance of the environment. In the case of MWNTs, $Z$ is assumed to be the characteristic impedance of the CNT given by Eq. (3.2) with $4M$ conducting channels. It was found in Ref. [P5] that the measured MWNTs have characteristic impedance of $Z = 1.3-7.7\,k\Omega$ and a kinetic inductance of $L_K = 0.1-4.2$ nH. The values were compared with the theoretical estimation providing evidence that 8 layers or bands are participating in the conduction. The value indicates that every third layer is conducting.

## 3.2 Carbon nanotube single electron transistor

The first reports on single-electron charging effects in individual singlewalled CNTs [57] and on bundles of singlewalled CNTs [23] were published in 1997. For singlewalled CNTs, the estimate for the Coulomb charging energy due to the self-capacitance $C_0$ is $e^2/\epsilon_0\epsilon L = 5$ meV$/(L\ [\mu\text{m}])$ on a silicon-dioxide substrate [58], where $L$ is the tube length. Singlewalled CNTs have shown charging energies of 30 meV, that is $\sim$ 300 K in temperature [58]. These CNTs with high charging energy are typically high-impedance devices $\gtrsim 1$ M$\Omega$. This is mostly due to the fact that an increase of the contact area between the CNT and the metal electrode lowers the resistance but increases the capacitance and thus also reduces the charging energy [59].

The first published results, to our knowledge, on Coulomb-charging effects on MWNTs are reported in Ref. [P2] . Papers [P2–P4] report experiments on three different MWNT SETs. All CNTs were produced with the arc-discharge method at the University Montpellier II. Measurements of these devices were done inside a plastic dilution refrigerator [40] at its base temperature of 80–120 mK.

Papers [P2,P6] report an experiment where a MWNT was positioned over two gold electrodes using AFM manipulation. The CNT was 410 nm long and had a diameter of 20 nm. There was a separate side-gate. The measured $IV$ curves as a function of gate voltage $V_g$ addressed that the CNT was semiconducting with a charging energy $E_C$ of 24 K. The asymmetric $IV_g$ curves implied an asymmetry in the tunnel-junction resistances and capacitances. Results of the measurement were explained by the Coulomb staircase

model [60, 61]. The asymmetry of the contact area between the CNT and the gold electrodes is also obvious in the AFM images. In this configuration, the higher-resistance tunnel junction between the CNT and the gold electrode dominates the conduction. This configuration is similar to the scanning tunnelling microscope (STM) spectroscopy for probing the density of states in carbon nanotubes [21, 22]. Figure 4 in Ref. [P6] displays the differential conductance of the measured $IV$ curve that is proportional to the density of states of the CNT.

The device, demonstrated in Ref. [P2] , was the first AFM manipulated CNT SET and one of the first experiments to build nanometer-scale electronic devices using AFM manipulation. The fabrication method was similar to the previous experiments, where nanoparticles had been moved with AFM in order to build an electronic point contact [62].

The experiment reported in Ref. [P3] utilized AFM manipulation to fabricate a SET made of two crossing MWNTs. In this experiment, MWNTs were first manipulated and electrodes were deposited over the tubes afterwards. The MWNT was in a direct contact with the substrate, unlike in the experiments of Refs. [P2,P3]. This experiment demonstrated one way to increase the gate capacitance and the possibility to use AFM to make more complicated structures. The measured charge noise of this device was $6{\times}10^{-4}$ e/$\sqrt{\text{Hz}}$ at 10 Hz, which corresponds to a typical metallic SET limited by $1/f$ noise due to conductance fluctuations at tunnelling barriers [63] or due to background charge fluctuations [64].

The freestanding MWNT SET reported in Ref. [P4] was fabricated using AFM manipulation. The contact resistance was lowered by vacuum brazing the sample at 700 °C. Figure 3.1 displays an AFM image of the device and a schematic of the sample geometry. The charge noise measured in this device had a value $6{\times}10^{-6}$ e/$\sqrt{\text{Hz}}$ at 45 Hz. The noise spectrum in Fig. 2 of Ref. [P4] is most probably due to the back-action of the current preamplifier voltage noise. Thus, the measured values are maximum estimates and the MWNT may have an even better charge sensitivity. This maximum estimate is of the same order as the best value reported for a metallic SET with stacked design [63]. In both of these designs, the SET island is further away from the background charge fluctuators of the substrate, and thus their contribution to charge noise is smaller. Another possible explanation for the enhanced

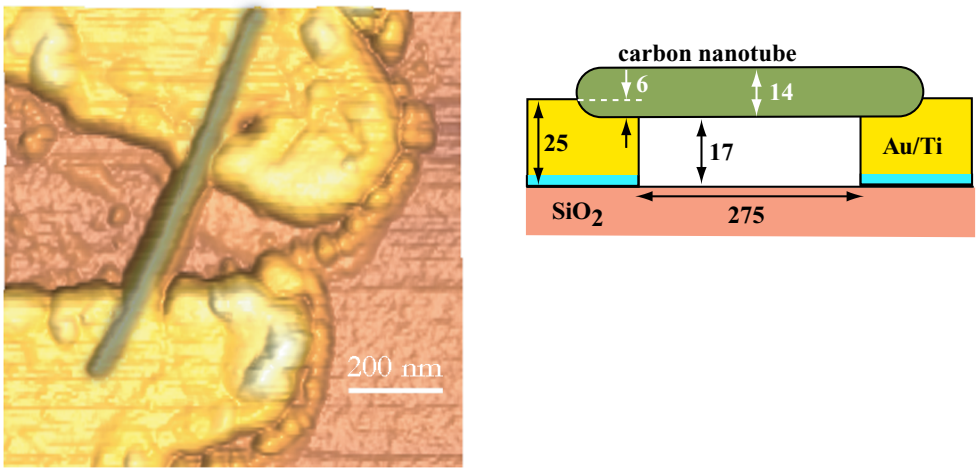


Figure 3.1: Left: AFM topography image of the MWNT measured in Ref. [P4]. Right: Sketch of the sample geometry. The dimensions are given in nanometers.

sensitivity is that during the AFM manipulation the amount of dirt on the surface of the MWNT is reduced. This is obvious from the AFM images taken during the manipulation process; The amount of dirt on a clean surface is sometimes increased after a MWNT has been moved over it.

As a further proof opposing the believed universality of $1/f$ charge fluctuations limit of $3\times10^{-4}$ e/$\sqrt{\text{Hz}}$ at 10 Hz [11], we made charge noise measurements with another MWNT sample fabricated with a similar method as in Ref. [P4]. The measurement was done using square-wave modulation as illustrated and explained in Fig. 3.2. The results are displayed in Fig. 3.3 and they show a value of $7\times10^{-5}$ e/$\sqrt{\text{Hz}}$ at 10 Hz.

The ultimate sensitivity of a SET is set by the shot noise. An estimate of the absolute minimum of the charge noise is $\delta Q_{min} \simeq \sqrt{\hbar C_\Sigma R_Q/4R}$ [66], where $R$ is the resistance of a single tunnel junction. The use of this estimate for the parameters of the sample in Ref. [P4] yield a shot-noise limited sensitivity of $4\times10^{-7}$ e/$\sqrt{\text{Hz}}$. In practice, temperature imposes the most severe restrictions for the SET sensitivity. This is due to the fact that small $C_\Sigma$ requires a small size island. On the other hand, a small island volume restricts the heat flow of the dissipated power out of the electron system in the island. The island temperature $T_i$ is related to the dissipated power $P$ over the SET

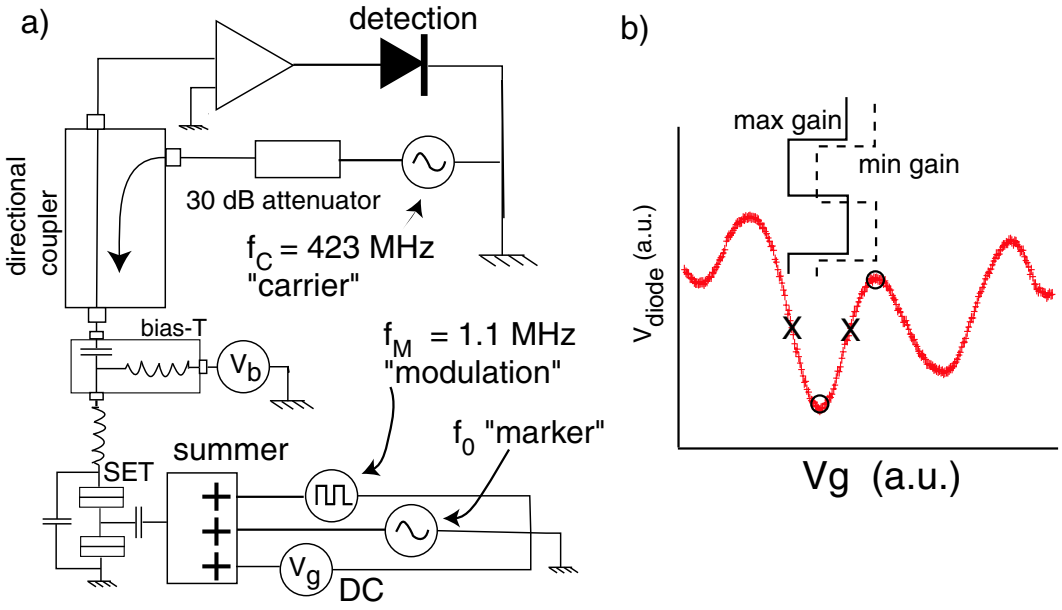


Figure 3.2: a) Square-wave modulated [65] RF-SET setup to detect $1/f$ noise in the MWNT. A square wave with frequency $f_M = 1.1$ MHz is applied to the gate electrode to AC bias the SET either between the maximum or the minimum charge-sensitivity points. These points have opposite slopes $dV_{\text{out}}/dV_g$ as illustrated in b). A marker signal with frequency $f_0$ with known island charge variation is applied to the gate at each frequency interval measured in order to scale the noise-floor to units of $\text{e}/\sqrt{\text{Hz}}$. A carrier of frequency $f_C$ = 423 MHz is used to transmit the signal as an amplitude modulation. b) Measured DC signal power with respect to the $V_g$ in order to find AC bias points.

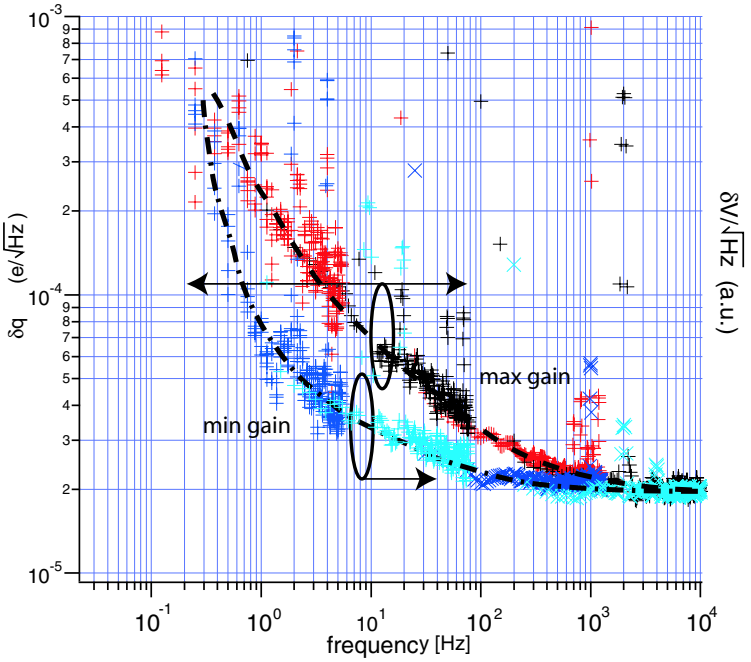


Figure 3.3: $1/f$ noise at the best charge-sensitivity points (around the dashed line) and worst charge-sensitivity points (around the dash-dotted line). The marker signals for the charge calibration, as explained in the caption of Fig. 3.2, are visible. Lines are to be taken as guides for the eyes. For the measurement setup, see Fig. 3.2. The charge sensitivity scale is only for the points of the best charge sensitivity. The constant noise at frequencies above 1 kHz is due to the preamplifier noise.

and the bath temperature $T_m$ via the relation $T_i^5 \approx T_m^5 + P/2\Sigma\Omega$, where $\Sigma$ is a constant of order 0.2 nW/(K$^5\mu$m$^3$) and $\Omega$ is the island volume [67]. This relation seems to hold also for the CNTs [68]. For a thermally limited symmetric SET, the charge sensitivity has an estimate $\delta Q_{min} \simeq 5.4(C_\Sigma/2)\sqrt{k_B T R}$ [66]. Using the dissipated power $P$ of $\sim$ 0.1 pW at the bias point and MWNT volume of $\Omega = (7\text{ nm})^2\pi \times 1\ \mu$m, we find the island temperature $T_i \simeq 1.2$ K, an order of magnitude higher than the bath temperature. We find the theoretical temperature-limited charge sensitivity of $7\times10^{-7}$ e/$\sqrt{\text{Hz}}$.

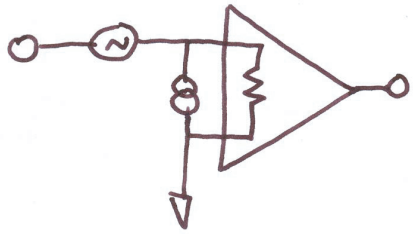

# Chapter 4

# Cryogenic high-frequency amplifier

THE first thing to do in the design of a low-noise rf-amplifier is the selection of an active element with the lowest noise temperature with sufficient gain. Once the active device and the operation point have been selected, other passive components are needed to transform the input and output ports of the active device to the right input and output impedances of the amplifier, that is, often to 50 Ω at high frequencies. This transformation can only increase the amplifier noise temperature from its internal minimum. Particularly, the dissipation at the amplifier input increases the amplifier noise temperature. There is also a chance that with unsuitable components the amplifier starts to oscillate. The design process of an amplifier is an optimization problem, in which one has to make trade-offs between the wanted amplifier input and output impedances, bandwidth, gain and noise temperature, with the boundary condition that the amplifier does not oscillate. At high frequencies it is difficult to split the design process into objects that fulfill boundary conditions. In my experience, it is no easy matter to understand how a variation of a component value affects the performance of the whole circuit. The effect is often opposite to the presumed one. Therefore, I followed the tradition to design the amplifiers en bloc as reported in Ref. [P9] . I selected an active device, bias point and circuit topology. Then I used an optimization algorithm to vary the circuit parameters in order to find the global minimum for the design goals.

The reason I devised an amplifier was that no commercial small cryogenic low-noise rf-amplifiers could be found and we needed one for the RF-SET system. I designed two amplifiers. The first amplifier was designed to be attached to a dip-stick inside a vacuum can with an outer diameter of two inches. Figure 4.1a is a photograph of the first amplifier. It showed $\sim$ 20 dB gain and an insertion loss ($S_{11}$) less than -10 dB in the band of 750–950 MHz. Its noise temperature was measured using the two-point Y method [17] and was found to be $\sim$7 K.

Paper [P9] reports the details of the design process for the second amplifier. It went as follows. A pseudomorphic High Electron Mobility Transistor (pHEMT) ATF35143 was selected due to its outstanding noise properties. The scattering parameters $S_{ij}$ (the complex 2 $\times$ 2 matrix) of the pHEMT were measured at different bias voltages at a temperature of 4.2 K. A scattering parameter $S_{ij}$ gives the complex voltage wave amplitude at port $j$, when port $i$ is excited with a voltage wave. As an example, $S_{21}$ is the gain $V_{out}/V_{in}$ if port 2 and 1 are output and input ports, respectively. The TRL calibration method was used to correct the effect of the cables and connectors from the network analyzer to the pHEMT [69]. Two-dimensional polynomial fits were done to the measured quantities $S_{ij}(V_{ds}, V_{gs})$, where $V_{ds}$ is the drain-source bias voltage and $V_{gs}$ the gate bias voltage. A bias point was selected with reasonable power dissipation and gain. The parameters of a small-signal circuit were fitted to give equivalent results with the scattering parameters. Effective temperatures were given to the components. By using the Pospiezalski noise model [70], all passive components were assumed to be at temperature of 5 K and the pHEMT channel temperature was assumed to be a factor four lower [71] than the reported room-temperature value [72]. After this process we had S-parameters (2 $\times$ 2 complex matrix) and the noise parameters (four real numbers) to describe the properties of the pHEMT at 4.2 K for any frequency between 400 MHz and 2400 MHz. Using these parameters, the full amplifier circuits in the balanced configuration [73] was designed by using numerical optimization.

The whole process was implemented by using Aplac software [74]. After the design process, the amplifier prototype was built. However, it feature oscillations around 12 GHz, where the pHEMT could not be modelled due to the limited frequency range of the characterization. After tuning of the cir-

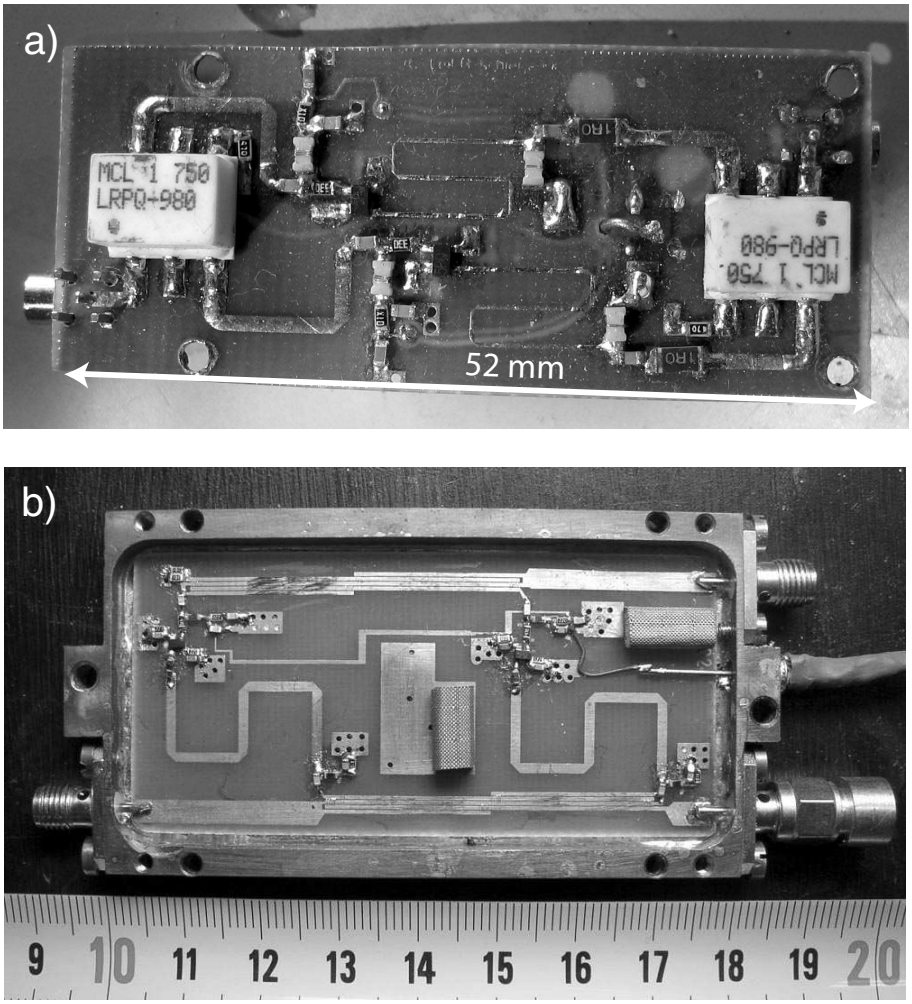


Figure 4.1: Photograph of the first amplifier a) and of the second amplifier b). The reduction of the dimensions in a) is achieved by using commercial hybrids (the white blocks). In b) the hybrids are implemented with the stripline Lange couplers. The input and output connections are implemented by using MMCX connectors in a) and by using SMA connectors in b). The design and characterization process of the amplifier in b) was reported in Ref. [P9] . The scale in b) is given in centimeters.

cuit parameters, the amplifier became stable and the new circuit parameters agreed with a new simulation [P9]. Finally, the amplifier noise properties were measured at 4.2 K and it showed a gain of $\sim$ 16 dB and a noise temperature $T_0 \sim 3$ K that is close to the best values reported [16]. According to the modelled noise parameters of ATF35143, it in theory is possible to construct a narrow-band amplifier with 50 $\Omega$ input and output impedances having noise temperature below 0.5 K over some limited frequency span below 1 GHz. The same pHEMT model has recently been used to build a low-temperature amplifier with the noise temperature $T_0 \sim$100 mK at an ambient temperature of 380 mK working in the frequency range 1–4 MHz [75].

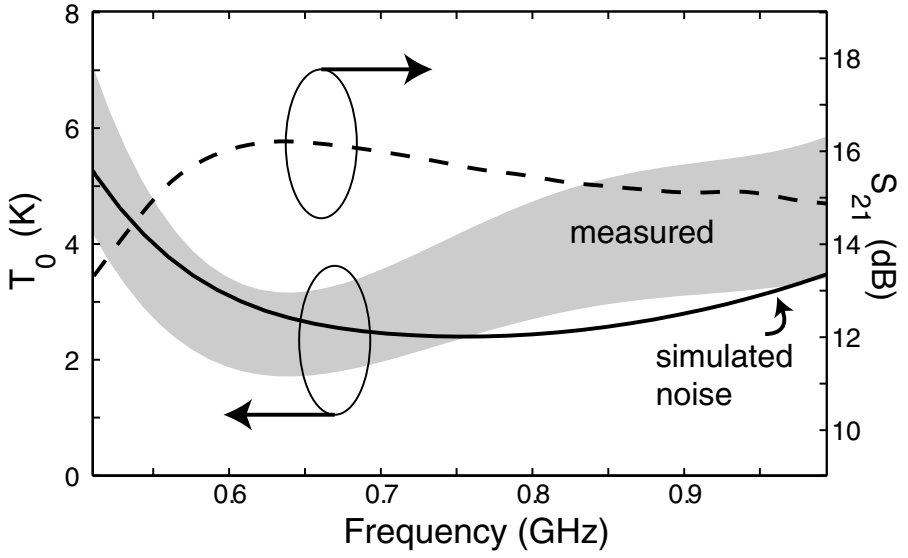


Figure 4.2: Measured noise temperature $T_0$ with error estimate (gray area) and the result from the simulation (solid line). The amplifier gain $S_{21}$ is denoted by the dashed line.

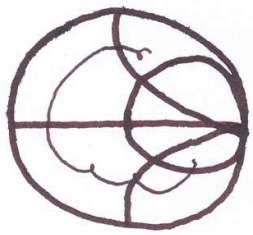

# Chapter 5

# Radio-frequency single-electron transistor

THE basic principle of the RF-SET is illustrated in Fig. 5.1a. A carrier wave is reflected from the impedance transformer circuit and the SET. The variation of the island charge changes the impedance of the SET and the reflected wave is amplitude modulated according to these changes. The optimal charge sensitivity is achieved with a perfect power match between the SET and the wave impedance of the transmission line. The SET bandwidth is limited by the loaded Q-factor of the impedance transformer. The theoretical maximum bandwidth may be studied with the help of the Bode-Fano criterion. It states that a resistor $R$ shunted by a capacitance $C$ may be matched to an arbitrary impedance by a lossless matching network with the following constraint [17]

$$\int_0^\infty \ln \frac{1}{|\Gamma(\omega)|} d\omega \leq \frac{\pi}{RC}, \tag{5.1}$$

where $\Gamma(\omega)$ is the reflection coefficient looking into the matching network according to Fig. 5.1b. The reflection coefficient characterized the relations between the incoming and reflected wave. For linear network $\Gamma$ may be written in terms of impedances

$$\Gamma = \frac{Z - Z_L}{Z + Z_L}. \tag{5.2}$$

As a simple example closely related to the RF-SET, if one built a matching network that had $\Gamma(\omega) = 0.1$ inside a limited band $\Delta\omega$, and $\Gamma(\omega) = 1$

elsewhere, it would follow that $\Delta\omega \leq \pi/(2.3RC)$. In other words, inside the frequency band $\Delta\omega \lesssim 1.36/RC$ power may be exchanged between the $RC$ circuit and the external impedance. Because the best charge sensitivity is attained when $\Gamma$ is close to zero, the shunting capacitance $C$ should be as small as possible in order to maximize $\Delta\omega$. In practice, the capacitance value is set by the bonding pad size of the SET chip and it is on the order of $\gtrsim 0.2$ pF. Consequently, the theoretical maximum bandwidth is $\sim 140$ MHz with good match ($\Gamma = 0.1$), $C = 0.2$ pF and $R = 50$ k$\Omega$. In order to understand the matching, it is useful to define the transforming impedance $Z_T \equiv 1/\omega_0 C$, where $\omega_0 = 1/\sqrt{LC}$. The $LC$-circuit transforms the SET resistance $R$ to a value $Z_T^2/R$. Therefore, $C$ should be $\sim$0.15 pF at 500 MHz in order to have a good match between 50 k$\Omega$ SET and a 50 $\Omega$ load impedance.

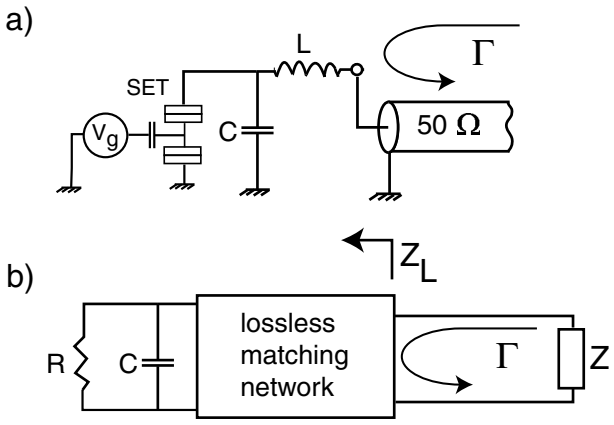


Figure 5.1: a) RF-SET configuration; a high impedance SET is matched with an $LC$-resonator to the 50 $\Omega$ transmission line. b) A matched RC circuit for the Bode-Fano criteria of Eq. (5.1). If $\Gamma = 1$ ($\Gamma = 0$), then no (all available) power is exchanged between the impedances $Z$ and $Z_L$.

Paper [P8] develops a full model of the RF-SET system, including matching circuit parasitics and the amplifier noise. It is used for a detailed experimental and theoretical analysis on the limitations of the charge sensitivity of the RF-SET setup. The analysis does not take into account the shot-noise in the SET, but assumes that there exists a lower bound due to the shot-noise $\sim 10^{-6}$ e/$\sqrt{\text{Hz}}$, as calculated in Ref. [19]. The starting point

is that a voltage wave with amplitude $v_0$ with a frequency $\omega_0$ is reflected from the SET-$LC$-circuit combination. The reflected wave has an amplitude $v_0[\Gamma_0 + \Delta\Gamma\cos(\omega_m t)]\cos(\omega_0 t) + n(t)$. Here $\Gamma_0$ is the reflection coefficient that is modulated with a sinusoidal modulation $\Delta\Gamma\cos(\omega_m t)$ that is due to the gate charge modulation $\propto \cos(\omega_m t)$. Above, $n(t)$ is the voltage noise of the reflected signal due to the amplifier noise over the amplifier input impedance. It is shown in Ref. [P8] that root-mean-square (rms) charge sensitivity is given by

$$\delta q_{\mathrm{rms}} = \frac{\sqrt{2S_V}}{v_0 \partial|\Gamma|/\partial q}, \tag{5.3}$$

where $S_V$ is the voltage spectral density of the noise term $n(t)$. Equation (5.3) was compared with the measurements of an aluminum SET in Ref. [P8] . The results agreed within 20 %.

By using Eq. (5.3) and a set of SET current-voltage curves with respect to the gate charge calculated with "orthodox" theory it was found that the charge sensitivity could be expressed with a simple phenomenological formula

$$\delta q \approx 1.46 \times 10^{-6} Z_T^{-0.91} t^{0.59} T_{EC}^{-1.01} R_\Sigma^{0.91} T_0^{0.5}. \tag{5.4}$$

$T_{EC}$ is the SET charging energy $E_C$ in Kelvins, $t$ is the island electron reduced temperature: $T_e$ divided by $T_{EC}$, $R_\Sigma$ is the total SET high-bias resistance in Ohms and $T_0$ is the total noise at the amplifier input in Kelvins. Eq. (5.4) reproduces the numerical results over $0.01 < t < 0.3$, $200 < Z_T < 2500$, $50k\Omega < R_N < 200k\Omega$ with a 50 % tolerance. It is to be taken strictly as a way to compress the sensitivity results into a single formula in the specified range of parameters.

The heating power of the AC bias voltage was calculated in order to estimate the real temperature of the SET island. The effective temperature was assumed to be described with the model $T_{\mathrm{eff}} \sim (P/(2\Sigma\Omega))^{1/5}$ [67], where $\Sigma$ is a constant of order $\sim 1$ nW/K$^5/\mu$m$^3$ and $\Omega$ is the volume of the SET island. It was found that the effective temperature for a typical metallic SET with an approximated island volume of $1\times0.2\times0.05$ $\mu$m$^3$ could be reproduced with the equation

$$T_{\mathrm{eff}} \approx 2.45 \times T_{EC}^{0.4} R_\Sigma^{-0.2}. \tag{5.5}$$

Combination of Eqs. (5.4) and (5.5) gives estimation for the charge sensitivity

$\delta q$ at the optimum operation point for a typical metallic SET

$$\delta q \approx 2.48 \times 10^{-6} Z_T^{-0.91} T_{EC}^{-1.3} R_\Sigma^{0.79} T_0^{0.5}. \quad (5.6)$$

Equation (5.6) was compared with the same measurements of the aluminum SET as above. The results agreed within 30 %. Experimental results found from the literature and the measured sensitivity of a MWNT were compared to the estimation Eq. (5.4), and fair agreement was found. It is to be noted that, in practical measurements, the parameters $T_0$ and $Z_T$ are not known very accurately due to the problem of accurate characterization of the line between the SET and the amplifier input. With the aluminum RF-SET discussed in Ref. [P8] , these parameters were carefully extracted. In the case of the MWNT RF-SET, the calibration of $T_0$ has to rely on separate measurements due to the properties of the shot noise that are not well established and may be sample-specific for MWNTs.

If the RF-SET is DC biased, the shot-noise-limited sensitivity may be enhanced through some fraction by applying an AC bias at the second harmonic of the carrier frequency. This result follows by applying the analysis of cyclostationary shot noise of Ref. [76] to the RF-SET system.

## 5.1 Carbon nanotube RF-SET

According to Eq. (5.4), a high charging energy enhances the RF-SET sensitivity. As was demonstrated in Ref. [P2] , MWNTs can be used to construct a SET with high charging energy. MWNTs have a volume smaller by a factor ∼100–1000 compared with metallic SET islands and thus their electron temperature increases to a higher value at the same dissipated power level, assuming the same electron-phonon coupling coefficient. This increase of temperature decreases the MWNT RF-SET sensitivity by 70–120 % according to Eq. (5.4) compared with a metallic device with a similar $E_C$. It is, however, easier to fabricate a SET with $E_C \geq 10$ K by using a MWNT as an island than making a similar metallic device using standard electron-beam lithography.

The major advantages of the RF-SET read-out are wide bandwidth and high charge sensitivity. The wide bandwidth means, in practice, that also conductance measurements may be carried out orders of magnitude faster

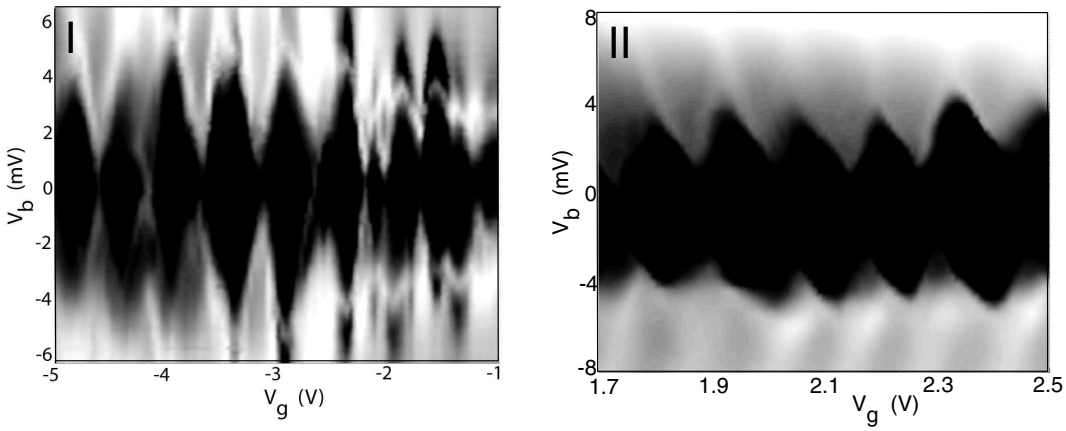


Figure 5.2: Reflected wave amplitude on a logarithmic scale, $\log(|\Gamma|)$, as a function of the gate and bias voltages. The lighter the color, the lower the reflection coefficient $|\Gamma|$. The MWNT samples were produced with plasma-enhanced CVD. The sample properties are listed in Table 5.1.

Table 5.1: Properties of the MWNT RF-SET samples I, II and III. Estimations for the charge sensitivity $\delta q$ are calculated using Eq. (5.4) and scaled with Eq. (5.5), taking into account the reduced CNT volume. The parameters $Z_T$ and $T_0$ for the samples I and II may contain a large error and must be taken with caution due to the malfunction of the directional coupler that was found out after the measurements.

| sample | I | II | III |
|---|---|---|---|
| electrodes | over CNT | under CNT | under CNT |
| AFM manipulated | no | yes | yes |
| diameter | 4 nm | 12 nm | 16 nm |
| $R_\Sigma$ | 125 kΩ | 400 kΩ | 150 kΩ |
| $T_{EC}$ | 20 K | 20 K | 3.5 K |
| $T_0$ | 5 K | 10 K | 4 K |
| length | 1.4 $\mu$m | 1.1 $\mu$m | 0.8 $\mu$m |
| $Z_T$ | 812 Ω | 637 Ω | 900 Ω |
| estimated $\delta q$ | $4.7\times10^{-6}e/\sqrt{\text{Hz}}$ | $1.7\times10^{-5}e/\sqrt{\text{Hz}}$ | $4.0\times10^{-5}e/\sqrt{\text{Hz}}$ |
| measured $\delta q$ | $1.6\times10^{-5}e/\sqrt{\text{Hz}}$ | $1.9\times10^{-5}e/\sqrt{\text{Hz}}$ | $1.86\times10^{-5}e/\sqrt{\text{Hz}}$ |

compared with the conventional low-frequency lock-in technique. The measurement is done in a fashion similar to the charge measurement of the RF-SET by reflecting a wave from the sample, but at a lower excitation level. The reflected wave amplitude is related to the sample impedance through Eq.(5.2), where $Z$ is the total impedance of the SET and $LC$-circuit combination and $Z_0$ is the characteristic impedance of the reflected wave.

The high-frequency setup discussed in Sec. 2.1 was employed to measure two MWNT samples, denoted by I and II, that showed reasonable Coulomb-charging diamonds. The sample parameters are listed in Table 5.1. The measurement setup and results for sample III are discussed in Ref. [P8]. Figure 5.2 depicts two graphs illustrating the reflected wave amplitude as a function of gate and bias voltages. The rhombic patterns are not as symmetric as in the case of metallic SETs, but the Coulomb-charging diamonds are obvious. In Fig. 5.2b, the tube features a gap in the conduction around zero bias, probably due to the semiconducting band structure. Most of the other measured MWNT samples did not show symmetric patterns. We measured the charge sensitivities by injecting a known small AC charge variation in the gate and optimized the carrier AC amplitude and gate DC bias point to give the highest charge resolution. The values of the measured charge sensitivities are listed in Table 5.1. The values estimated using Eq. (5.4) and volumes scaled according to Eq. (5.5) agree moderately well with the measured ones.

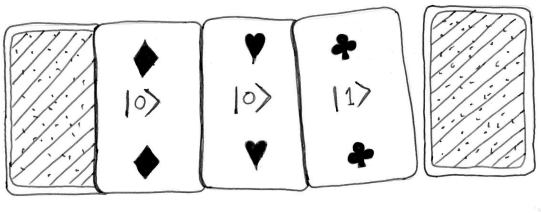


# Chapter 6

# Discussion

THIS Thesis deals with CNTs and their use as single-electron transistors. The possibility to build SETs out of MWNTs has been demonstrated. The measured MWNT SET showed a high charge sensitivity. Good sensitivity means that a signal can be read fast. The difference between the sensitivities $10^{-6}e/\sqrt{\text{Hz}}$ and $10^{-5}e/\sqrt{\text{Hz}}$ is that, in the latter case, one needs to measure a hundred times longer time compared with the former case, in order to reach the same charge resolution. If the measurement time poses no problems, one should at the outset select the easiest and most reliable method.

If one were to make actual charge measurements using a SET today, one would probably select to use a device made of aluminum. The fact that the sample fabrication process, the materials properties and the results are reproducible, is vital for real applications. The CNTs can be used to fabricate SETs, but according to the experience in our group, it seems that every sample is an individual; there is the possibility for a CNT to have many different chiralities, the contact resistances may vary, and there occur impurities at random locations. The CNT samples are also more laborious to make than aluminum SET samples. There is, however, always the possibility that the fabrication methods of the CNTs will advance, and they may in fact become quite practical elements within nanoscale electronics in next 5–20 years. The task of this Thesis has been to take one of the first steps towards this direction.

The future of the nanoelectronics depends strongly on the progress of

novel fabrication techniques. The developed AFM manipulation methods, were used in practice to construct electrical components. The most severe problem of scanning probe manipulation is its relative slowness. Moreover, the tip degradation is fast compared with the plain topographic imaging. The AFM manipulation is, however, probably the best tool for the controlled positioning of nanometer-scale objects. Yet, it has been utilized relatively little in research.

Part of the experimental work of this Thesis handles the construction of the RF-SET measurement setup. The development of the high-frequency measurement system was a slow process, as is everything related to the low temperature physics. Conventionally, electrical transport measurements of refrigerated mesoscopic samples have consisted of measurements of current, voltage and conductance at low frequencies. These methods are well established and the last problem, the high frequency electro-magnetic environment around the sample, can be regulated by the use of an appropriate filtering.

The high-frequency measurements imply, in essence, enhanced time resolution for the measured quantities. An improved accuracy is sometimes achieved by using such high-frequency methods, in which $1/f$ noise has a negligible contribution. Fast measurements, like those in the RF-SET, typically feature a bandwidth of $\sim$10 MHz. This corresponds to a time resolution of 100 ns, a sufficient rate for certain types of solid-state quantum measurements. This branch of science, still struggling to build and control two coupled quantum bits, aims to develop techniques to realize a quantum computer in the future.

The RF-SET uses resistive readout. Another possibility is to use reactive readout. The use of Josephson-junction circuits with reactive readout enables one to read the charge or the quantum states in a less dissipative manner. The research conducted here in order to accomplish a high-frequency measurement system, constitutes the first step towards research on quantum measurements using novel read-out techniques. The measurement setup also makes it possible to measure noise accurately, in order to extract information – sometimes additional – about the physical phenomena under study.

# References

[1] T.A. Fulton and G.J. Dolan. Observation of single-electron charging effects in small tunnel junctions. *Phys. Rev. Lett.*, 59:109, 1987.

[2] S. Ijima. Helical microtubules of graphitic carbon. *Nature (London)*, 354:56, 1991.

[3] R.J. Schoelkopf, P. Wahlgren, A.A. Kozhevnikov, P. Delsing, and D.E. Prober. The radio-requency single-electron transistor (RF-SET): A fast and ultrasensitive electrometer. *Science*, 280:1238, 1998.

[4] Peter Wahlgren. *The Radio Frequency Single-Electron Transistor and the Horizon Picture for Tunneling*. PhD thesis, Chalmers University of Technology, 1998.

[5] Alexander N. Korotkov. Coulomb blockade and digital single-electron devices. In J. Jortner and M.A. Ratner, editors, *Molecular Electronics*. Blackwell, Oxford, 1998.

[6] C.J. Gorter. A possible explanation of the increase of the electrical resistance of thin metal films at low temperatures and small field strengths. *Physica*, 17:777, 1951.

[7] C.A. Neugebauer and M.B. Webb. Electrical conduction mechanism in ultrathin, evaporated metal films. *J. Appl. Phys.*, 33:74, 1962.

[8] K. K. Likharev. Single electron devices and their applications. *P. IEEE*, 87:606, 1999.

[9] D. V. Averin and K. K. Likharev. Single electronics: A correlated transfer of single electrons and Cooper pairs in systems of small tunnel junc-

tions. In B. L. Altshuler, P. A. Lee, and R. A. Webb, editors, *Mesoscopic Phenomena in Solids*, page 173. Elsevier, 1991.

[10] G.L. Ingold and Yu.V. Nazarov. Charge tunneling rates in ultrasmall junctions. In H. Grabert and M.H. Devoret, editors, *Single Charge Tunneling*. Plenum Press, N.Y., 1992.

[11] V. Bouchiat. *Quantum fluctuations of the charge in single electron and single Cooper pair devices*. PhD thesis, CEA-Saclay, 1997.

[12] G. Zimmerli, R.L. Kautz, and J.M. Martinis. Voltage gain in the single electron transistor. *Appl. Phys. Lett.*, 61:2616, 1992.

[13] Analog Devices, AD797 Technical Data.

[14] H. Rothe and W. Dahlke. Theory of noisy fourpoles. *Proc. IRE*, 44:811, 1956.

[15] J. Engberg and T. Larsen. *Noise Theory of Linear and Nonlinear Circuits*. John Wiley, New York, 1995.

[16] R. F. Bradley. Cryogenic, low-noise, balanced amplifiers for the 300–1200 MHz band using heterostructure field-effect transistors. *Nucl. Phys. B*, 72:137, 1999.

[17] D. M. Pozar. *Microwave engineering*. Addison-Wesley, New York, 1st edition, 1990.

[18] C.M. Caves. Quantum limits on noise in linear amplifiers. *Phys. Rev. D*, 26:1817, 1982.

[19] A.N. Korotkov and M.A. Paalanen. Charge sensitivity of radio frequency single-electron transistor. *Appl. Phys. Lett.*, 74:4052–4054, 1999.

[20] R. Saito, G. Dresselhaus, and M.S. Dresselhaus. *Physical Properties of Carbon Nanotubes*. Imperial College Press, London, 1998.

[21] J.W.G. Wildöer, L.C. Venema, A.G. Rinzler, R.E. Smalley, and C. Dekker. Electronic structure of atomically resolved carbon nanotubes. *Nature (London)*, 391:59, 1998.

[22] T.W. Odom, J.-L. Huang, P. Kim, and C.M. Lieber. Atomic structure and electronic properties of single-walled carbon nanotubes. *Nature (London)*, 391:62, 1998.

[23] M. Bockrath, D.H. Cobden, P.L. McEuen, N.G. Chopra, A. Zettl, A. Thess, and R.E. Smalley. Single-Electron Transport in Ropes of Carbon Nanotubes. *Science*, 275:1922, 1997.

[24] J. Nygård, D.H. Cobden, and P.E. Lindelöf. Kondo physics in carbon nanotubes. *Nature (London)*, 408:342, 2000.

[25] S. Frank, P. Poncharal, Z.L. Wang, and W.A. de Heer. Carbon nanotube quantum resistors. *Science*, 280:1744, 1998.

[26] P. Poncharal, C. Berger, Y. Yi, Z.L. Lang, and W.A. de Heer. Room temperature ballistic conduction in carbon nanotubes. *J. Phys. Chem. B*, 106:12104, 2002.

[27] A.Y. Kasumov, R. Deblock, M. Kociak, B. Reulet, H. Bouchiat, I.I. Khodos, Yu.B. Gorbatov, V.T. Volkov, C. Journet, and M. Burghard. Carbon nanotubes as molecular quantum wires. *Science*, 284:1508, 1999.

[28] M. Kociak, A.Y. Kasumov, S. Gueron, B. Reulet, I.I. Khodos, Y.B. Gorbatov, V.T. Volkov, L. Vaccarini, and H. Bouchiat. Superconductivity in ropes of single-walled carbon nanotubes. *Phys. Rev. Lett.*, 86:2416, 2001.

[29] P.G. Collins, M.S. Fuhrer, and A. Zettl. $1/f$ noise in carbon nanotubes. *Appl. Phys. Lett.*, 76:894, 2000.

[30] M. Bockrath, D.H. Cobden, J. Lu, A.G. Rinzler, R.E. Smalley, L. Balents, and P.L. McEuen. Luttinger-liquid behaviour in carbon nanotubes. *Nature (London)*, 397:598, 1999.

[31] C. Schönenberger, A. Bachtold, C. Strunk, J.-P. Salvetat, and L. Forro. *Phys. A: Mater. Sci. Process.*, 69:283, 1999.

[32] A. Bachtold, C. Strunk, J.-M. Bonard J.-P. Salvetat, L. Forro, T. Nussbauer, and C. Schönenberger and. Aharonov-bohm oscillations in carbon nanotubes. *Nature (London)*, 397:673, 1999.

[33] J. Nygård. *Experiments on Mesoscopic Electron Transport in Carbon Nanotubes*. PhD thesis, University of Copenhagen, 2000.

[34] C. Dekker. Carbon nanotubes as molecular quantum wires. *Physics Today*, May:22, 1999.

[35] J.W. Mintmire, B.I. Dunlap, and C.T. White. Are fullerene tubules metallic? *Phys. Rev. Lett.*, 68:631, 1992.

[36] N. Hamada, S. Sawada, and A. Oshiyama. New one-dimensional conductors: graphitic microtubules. *Phys. Rev. Lett*, 68:1579, 1992.

[37] R. Saito, M. Fujima, G. Dresselhaus, and M.S. Dresselhaus. Electronic structure of chiral graphene tubules. *Appl. Phys. Lett.*, 60:2204, 1992.

[38] P. R. Wallace. The band theory of graphite. *Phys. Rev.*, 71:622, 1947.

[39] J.J. Palacios, A.J. Pérez-Jiménez, E. Louis, E. SanFabián, and J.A. Vergés. First-principles phase-coherent transport in metallic nanotubes with realistic contacts. *Phys. Rev. Lett*, 90:6801, 2003.

[40] Nanoway PDR 50, Nanoway Oy, FIN-40500 Jyväskylä, Finland, www.nanoway.fi.

[41] Leiden Cryogenics MNK126-500, Leiden Cryogenics BV0, 2311 Leiden, The Netherlands, www.leidencryogenics.com.

[42] JC Nabity Lithography Systems, P.O.Box 5354, Bozeman, MT 59717 USA.

[43] MER Corporation, 7960 South Kolb Road, Tucson, Arizona 85706, USA.

[44] G. Binnig, C. Quate, and Ch. Gerber. Atomic force microscope. *Phys. Rev. Lett.*, 56:930, 1986.

[45] D. Eigler and E. K. Schweizer. Positioning single atoms with a scanning tunnelling microscope. *Nature (London)*, 344:524, 1990.

[46] T. Junno, K. Deppert, L. Montelius, and L. Samuelson. Controlled manipulation of nanoparticles with an atomic force microscope. *Appl. Phys. Lett.*, 66:3627, 1995.

[47] D.M. Schaefer, R. Reidenberger, A. Patil, and R.P. Andres. Fabrication of two-dimensional arrays of nanometer-size clusters with the atomic force microscope. *Appl. Phys. Lett.*, 66:1012, 1995.

[48] M.R. Falvo, G.J. Clary, R.M. Taylor, V. Chi, F.P. Brooks, S. Washburn, and R. Superfine. Bending and buckling of carbon nanotubes under large strain. *Nature (London)*, 389:582, 1997.

[49] T. Hertel, R. Martel, and P. Avouris. *J. Phys. Chem. B*, 102:910, 1998.

[50] M.R. Falvo, R.M. Taylor, A. Heiser, V. Chi, F.P. Brooks, S. Washburn, and R. Superfine. Nanometre-scale rolling and sliding of carbon nanotubes. *Nature (London)*, 397:236, 1999.

[51] R. Resch, A. Bugacov, C. Baur, B.E. Koel, A. Madhukar, A.A.G. Requicha, and P. Will. *Appl. Phys. A*, 67:265, 1998.

[52] P.J. de Pablo, J. Colchero, M. Luna, J. Gómez-Herrero, and A.M. Baró. Tip-sample interaction in tapping-mode scanning force microscopy. *Phys. Rev. B*, 61:14179, 2000.

[53] P.J. Burke. Luttinger liquid theory as a model of the gigahertz electrical properties of carbon nanotubes. *IEEE Trans. Nano.*, 1:129, 2002.

[54] E.B. Sonin. Tunneling into a 1d and quasi-1d conductors and Luttinger liquid behavior. *J. Low Temp. Phys.*, 124:321, 2001.

[55] J. Penttilä, Ü. Parts, P. Hakonen, M. Paalanen, and E. Sonin. Effect of quantum noise on Coulomb blockade in normal tunnel junctions at high voltages. *Phys. Rev. B*, 61:10890, 2000.

[56] J. Penttilä. *Influence of electromagnetic environment in single tunnel junctions.* PhD thesis, Helsinki University of Technology, 2001.

[57] S.J. Tans, M.H. Devoret, H. Dai, A. Thess, R.S. Smalley, L.J. Geerlings, and C. Dekker. Electron-electron correlations in carbon nanotubes. *Nature (London)*, 386:474, 1997.

[58] J. Nygård, D.H. Cobden, M. Bockrath, P.L. McEuen, and P.E. Lindelöf. Electrical transport measurements on single-walled carbon nanotubes. *Appl. Phys. A*, 69:297, 1999.

[59] K. Tsukagoshi, N. Yoneya, S. Uryu, Y. Aoyagi, A. Kanda, Y. Ootuka, and B.W. Alphenaar. Carbon nanotube devices for nanoelectronics. *Physica B*, 323:107, 2002.

[60] A.E. Hanna and M. Tinkham. Variation of the Coulomb staircase in a two-junction system by fractional electron charge. *Phys. Rev. B*, 44:5919, 1991.

[61] L. Roschier. Fabrication of single electron transistor using scanning probe manipulation. Master's thesis, Helsinki University of Technology, 1999.

[62] T. Junno, S.-B. Carlsson, H. Xu, L. Montelius, and L. Samuelson. Fabrication of quantum devices by Ångström-level manipulation of nanoparticles with an atomic force microscope. *Appl. Phys. Lett.*, 72:548, 1998.

[63] V. Krupenin, D. Presnov, M. Savvateev, H. Scherer, A. Zorin, and J. Niemeyer. Noise in Al single electron transistor of stacked design. *J. Appl. Phys.*, 84:3212, 1998.

[64] B. Starmark, T. Henning, T. Claeson, P. Delsing, and A.N. Korotkov. Gain dependence of the noise in the single electron transistor. *J. Appl. Phys.*, 86:2132, 1999.

[65] G. Zimmerli, T.M. Eiles, R.L. Kautz, and J.M. Martinis. Noise in the Coulomb blockade electrometer. *Appl. Phys. Lett.*, 61:237, 1992.

[66] A.N. Korotkov, D.V. Averin, K.K. Likharev, and S.A. Vasenko. Single-electron transistors as ultrasensitive electrometers. In H. Koch and H. Lübbig, editors, *Single-Electron Tunneling and Mesoscopic Devices*, page 45. Springer-Verlag, Berlin, 1992.

[67] R.L. Kautz, G. Zimmerli, and J.M. Martinis. Self-heating in the Coulomb-blockade electrometer. *J. Appl. Phys.*, 73:2386, 1993.

[68] R. Tarkiainen, M. Ahlskog, P. Hakonen, and M. Paalanen. Electron heating effects in disordered carbon nanotubes. *J. Phys. Soc. Jpn.*, 72:100, 2002.

[69] Hewlett-Packard Application note 1287–9.

[70] M. Pospiezalski. Modeling of noise parameters of MESFET's and MODFET's and their frequency and temperature dependence. *IEEE Trans. Microw. Theory*, 9:1340, 1989.

[71] J.W. Kooi, www.submm.caltech.edu/cso/receivers/papers/ballna.pdf.

[72] Agilent Technologies, ATF35143 Technical Data.

[73] K. Kurokawa. Design theory of balanced transistor amplifiers. *Bell Syst. Tech. J.*, 44:1675, 1965.

[74] Aplac Solutions Corporation, P.O. Box 284, FIN-02600 Espoo, Finland, www.aplac.com.

[75] N. Oukhanski, M. Grajcar, E. Il'chev, and H.-G. Meyer. Low noise, low power consumption high electron mobility transistors amplifier, for temperatures below 1 K. *Rev. Sci. Instrum.*, 74:1145, 2003.

[76] M. Rakhmanov. Demodulation of intensity and shot noise in the optical heterodyne detection of laser interferometers for gravitational waves. *Appl. Opt.*, 40:6596, 2001.